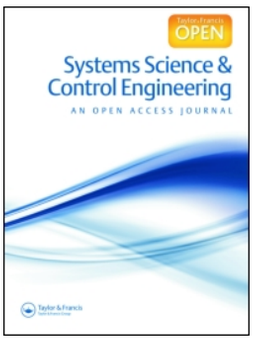

Systems Science & Control Engineering

An Open Access Journal

ISSN: (Print) 2164-2583 (Online) Journal homepage: http://www.tandfonline.com/loi/tssc20

Modulation signal bispectrum analysis of electric signals for the detection and diagnosis of compound faults in induction motors with sensorless drives

Abdulkarim Shaeboub, Fengshou Gu, Mark Lane, Usama Haba, Zhifei Wu & Andrew D. Ball

To cite this article: Abdulkarim Shaeboub, Fengshou Gu, Mark Lane, Usama Haba, Zhifei Wu & Andrew D. Ball (2017) Modulation signal bispectrum analysis of electric signals for the detection and diagnosis of compound faults in induction motors with sensorless drives, Systems Science & Control Engineering, 5:1, 252-267, DOI: 10.1080/21642583.2017.1331769

To link to this article: http://dx.doi.org/10.1080/21642583.2017.1331769

SYSTEMS SCIENCE & CONTROL ENGINEERING: AN OPEN ACCESS JOURNAL, 2017
VOL. 5, 252–267
https://doi.org/10.1080/21642583.2017.1331769

Taylor & Francis
Taylor & Francis Group

Modulation signal bispectrum analysis of electric signals for the detection and diagnosis of compound faults in induction motors with sensorless drives

Abdulkarim Shaeboub[a], Fengshou Gu[a,b], Mark Lane[a], Usama Haba[a], Zhifei Wu[b] and Andrew D. Ball[a]

[a]Centre of Efficiency and Performance Engineering, University of Huddersfield, Huddersfield, UK; [b]Department of Vehicle Engineering, Taiyuan University of Technology, Taiyuan, People's Republic of China

ABSTRACT

As a prime driver, induction motor is the most electric energy consuming component in industry. The exposure of the motor to stator winding asymmetry, combined with broken rotor bar fault significantly increases the temperature and reduces the efficiency and life of the motor. Accurate and timely diagnosis of these faults will help to maintain motors operating under optimal status and avoid excessive energy consumption and severe damages to systems. This paper examines the performance of diagnosing the effect of asymmetry stator winding on broken rotor bar (BRB) faults under closed loop operation modes. It examines the effectiveness of conventional diagnostic features in both motor current and voltage signals using spectrum and modulation signal bispectrum analysis (MSBA). Evaluation results show that the combined faults cause an additional increase in the sideband amplitude and this increase in sideband can be observed in both the current and voltage signals under the sensorless control mode. MSB analysis has a good noise reduction capability and produces a more accurate and reliable diagnosis in that it gives a more correct indication of the fault severity and its location for all operating conditions.

ARTICLE HISTORY
Received 14 January 2017
Accepted 15 May 2017

KEYWORDS
Induction motor; stator winding asymmetry and broken rotor bar; variable speed drive (VSD); motor current and voltage signatures analysis

Introduction

Induction motors are commonly mentioned as the workhorse of industries, mainly because of their simple yet powerful architectural construction, ergonomically adaptable structure, being rugged and highly robust and offering high value of reliability. However, they are prone to various faults related to their functionalities and operational environments. Such faults can cause not only the loss of production but also even catastrophic incidents and additional costs. Increases in signal stator resistance of a three phase induction motor can lead to voltage imbalances in the motor causing a reduction in motor efficiency, increases in motor temperature and oscillatory running conditions, which in turn can lead to other electrical or mechanical failures occurring. There are many reasons for stator winding asymmetry such as generators terminal voltages, load currents, faults, power factor correction equipment and voltage regulators in the utility distribution lines (Sridhar & Rao, 2013). However, this fault will remain undetected by the drive system because the motor is still functionally operational under these imbalanced conditions, albeit operating less efficiently. Even motor resistance imbalance applied to the motor is small, large unbalanced motor current can be flowed because of relatively low negative sequence impedance. The large unbalanced current creates difficult problems in induction motor applications such as a heat problem, increases of losses, vibrations, acoustic noises and shortening of life (Mirabbasi, Seifossadat, & Heidari, 2009). The maximum amplitude of the current and torque are significantly increased by increasing the stator winding asymmetry factor. Therefore, efficient and effective condition monitoring techniques are actively studied to detect the faults at an early stage in order to prevent any major failures on motors (Alwodai, Gu, & Ball, 2012; Hussein, Mahmood, & Abdulbaqi, 2011).

Of many different techniques in developing, motor current signature analysis (MCSA) has been found more effective and efficient in monitoring different motor faults including air-gap eccentricity, broken rotor bar and turn to turn fault in the stator. It is centred on using popular frequency analysis methods to diagnose current harmonics and sidebands at such frequencies that uniquely identify the features of relative faults. Moreover, it does not require any additional systems for measurements (Ashari, Lane, Gu, & Ball, 2014; El Hachemi Benbouzid, 2000) and can be implemented remotely at low investment.

CONTACT Fengshou Gu f.gu@hud.ac.uk

Vamvakari (Vamvakari, Kandianis, Kladas, Manias, & Tegopoulos, 2001) and Kersting (Kersting, 2001) have shown that the performance, efficiency and life of induction motors can be considerably affected by the quality of the power supply. Sharifi and Ebrahimi (Sharifi & Ebrahimi, 2011) developed a method for the diagnosis of inter-turn short circuit faults in the stator windings of induction motors. The technique is based on MCSA and utilizes three phase current spectra to overcome the problem of supply voltage unbalance. Flux and vibration analysis for the detection of stator winding faults in induction motor was presented (Lamim Filho, Pederiva, & Brito, 2014). Park-Hilbert (P-H) was introduced to diagnose stator faults in induction motors using grouping between the Hilbert transform and the Extended Park's Vector methodology (Sahraoui, Zouzou, Ghoggal, & Guedidi, 2010).

Higher order spectra (HOS) are useful signal processing tools that have shown significant benefits over traditional spectral analyses because HOS have unique properties of nonlinear system identification, phase information retention and Gaussian noise elimination (Gu, Shao, Hu, Naid, & Ball, 2011; Zhang, Gu, Mansaf, Wang, & Ball, 2017). Therefore, HOS analysis has received high concentrations. Study in (Gu et al., 2011) has researched the use of motor current signals for the diagnosis of different faults, has in reciprocating compressors revealed that by suppressing random noise with a new data processing method, namely modulation signal bispectrum (MSB), which is an extension of CB for analysing modulation signals particularly, has resulted in more accurate diagnosis than that of power spectrum (PS). More details on current signature analysis have been presented in (Gu et al., 2015) on the new improved BRB diagnosis based on modulation signal bispectrum analysis without the use of close loop control modes. The current signals on the healthy machine and under BRB are explained. The ideal electromagnetic relationship of the driving motor on both healthy and under BRB can be examined. The results are that the additional current with sinusoidal wave at frequency $2sf_s$ for the case of BRB can be found. Modulation signal bispectrum analysis of motor current signals is used for the detection of stator faults, which is presented by (Alwodai, Yuan, Shao, Gu, & Ball, 2012). These faults can cause winding temperature to increase which may have an effect on current signal. Results illustrated by (Alwodai, Yuan, et al., 2012) prove that MSB analysis has the potential to accurately and efficiently evaluate modulation degrees and overpower the random and non-modulation components. Another novel technique is used for the diagnosis of inter-turn short circuit fault in induction motor by (Ceban, Pusca, Romary, & Lecointe, 2011). This diagnostic technique is purely based on the analysis of external magnetic field in the surrounding area of the machine and more specifically its space deviations calculated by two coil sensors. The standard is based on the contrast of the particular harmonic magnitude whilst the machine runs with or without any load. Its major concentration is on the point that the load operation does not establish any more disturbing factor, but it fairly corresponds to a vital state allowing failure perception.

It is also common that two or more such faults may develop simultaneously, making it important to identify if they are alone or compound. Recently, the compound fault identification in induction motors represented a big challenge. Messaoudi and Sbita (Messaoudi & Sbita, 2010) used motor current spectrum to detect multiple faults in induction motors. The application of high-resolution spectral analysis for identifying multiple compound faults in induction motors developed by (Garcia-Perez, de Jesus Romero-Troncoso, Cabal-Yepez, & Osornio-Rios, 2011). The exposure of the motor to unbalanced supply, combined with broken rotor bar fault significantly increases the temperature and reduces the efficiency and consequently, the damage to the induction motor (Constantine, 2014; Sridhar & Rao, 2013). All the above mentioned works focus on fault detection of induction motors directly connected to the power line supply and do not discover the effects of close loop variable speed drive system on the power supply parameters, i.e. current and voltage in the case of induction motor faults which are increasingly used in industry for obtaining better dynamic response, higher efficiency and lower energy consumption. However, VSD systems can induce strong noise to voltage and current measurements.

The contributions of this paper present a new method for detecting and diagnosing combined faults of stator winding asymmetry and broken rotor bar using electrical signals from variable speed drive. Both the motor current and terminal voltage signals are examined with different degrees of severities and under sensorless control (close) modes operating under different loads. Moreover, both the common power spectrum and MSB analysis applied to these signals to benchmark their performances of diagnosing these faults.

This paper is structured as follows: Section 2, the performance of diagnostic features, effects of asymmetry stator winding and broken rotor bar faults are examined. Section 3, a new sideband amplitude estimator based on modulation signal bispectrum analysis is developed. Section 4 explains the principle of a VSD and how induction motor faults influence current and voltage in a VSD system and in this study the sensorless drive is considered as it is very commonly used in industries. Section 5, the test facilities, their specifications and rig operations are detailed along with the introduction of compound faults

into the motor. Section 6, the diagnosis results of the asymmetry stator winding and the broken rotor bar faults are examined under the closed loop operation mode.

Fault features and effects

Broken rotor bars

Broken Rotor Bar (BRB) and end-ring condition is one of the most common induction machine asymmetrical rotor and/or stator winding connections. This asymmetrical operation results in unbalanced air gap voltage, consequently unbalanced line currents, increased losses, increased torque pulsations and decrease in average torque. Of the most severe faults, it will result in reduced efficiency and excessive heating which eventually leads to the failure of the machine. Figure 1(a) and (b) show the equivalent circuits of the broken rotor bar detailing the rotor loop current and end ring current. Detailed calculations are proposed in (Alwodai, 2015).

There are unique characteristic frequencies of a broken rotor bar fault that can be measured at (Alwodai, Gu, et al., 2012):

$$f_{\text{brb}} = f_s(1 \pm 2ks), \quad k = 1, 2, 3, \ldots \tag{1}$$

The per unit slip s is calculated as follows:

$$s = \frac{f_s/p - f_r}{f_s/p} \tag{2}$$

where f_s denotes the frequency of supply, f_r is the speed of the rotor, p is the number of pole-pairs.

The sidebands that are around the supply frequency in Equation (1) are likely to be present in the phase current power spectrum. In the event of broken bars it can result in particular significance of the first-order sidebands ($k = 1$) for the diagnosis of broken rotor bar fault. While the right sideband $f_s(1 + 2ks)$ is due to the speed variation or ripple and the left sideband $f_s(1 - 2ks)$ is due to magnetic or electrical rotor asymmetry that is caused by the broken rotor bars. The presence and amplitudes of the sidebands are reliant on the physical position of the broken rotor bars as well as motor's load and speed.

Stator winding asymmetry

A small amount of motor resistance imbalance will cause an increase in the winding temperature by a large amount. As a general rule if the temperature rises by 25% (in °C) for every 3.5% voltage imbalance (Payne, 2003)

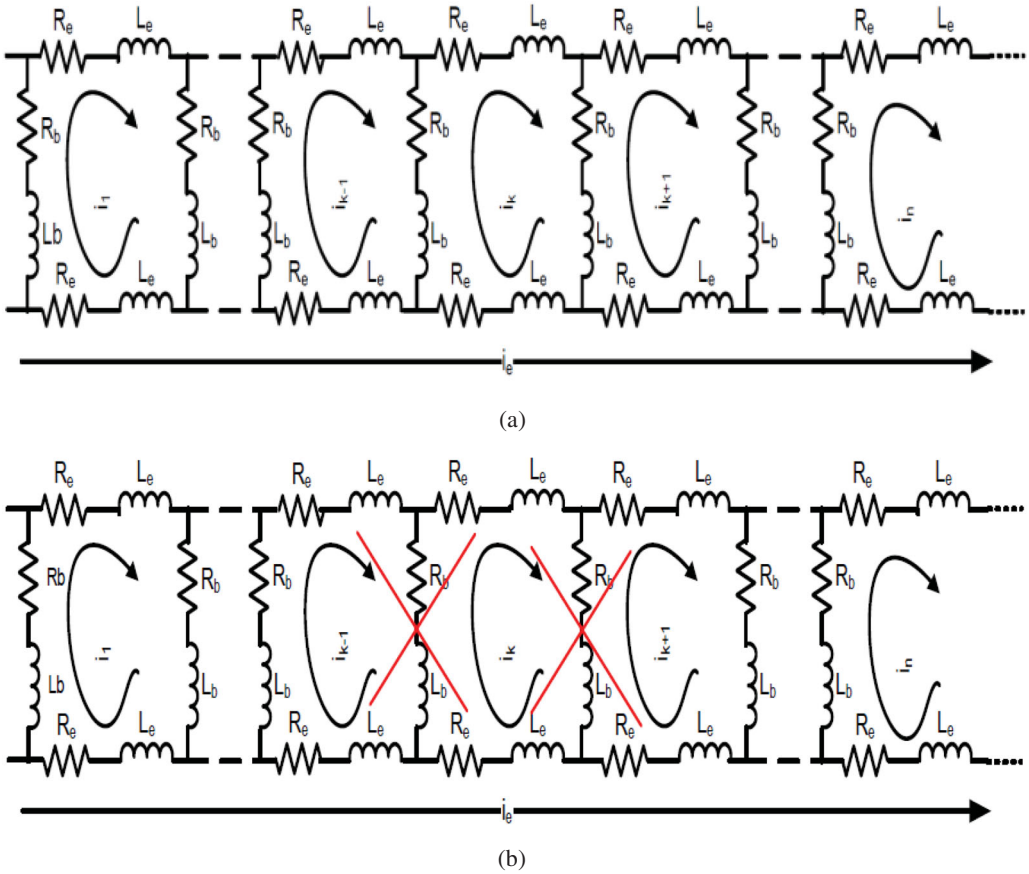

Figure 1. (a) Equivalent circuit of a rotor, (b) equivalent circuit of a rotor with two broken bars.

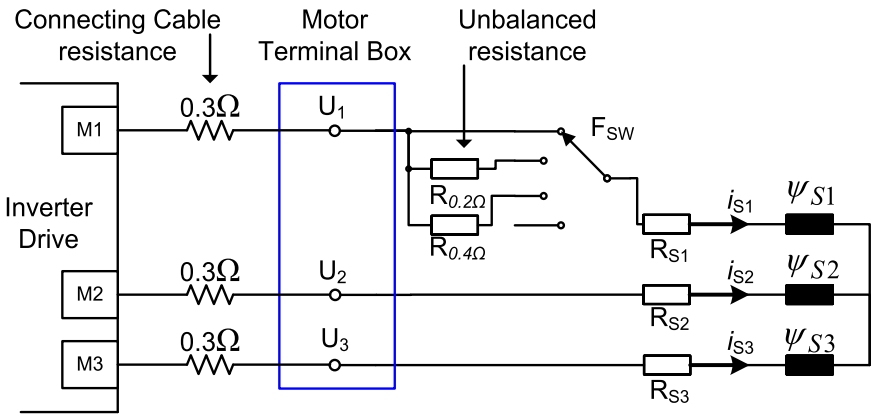

Figure 2. Asymmetry stator winding faults due to loose electric connection or winding shortages.

there is a 7% current imbalance expected for every 1% voltage imbalance, which is equivalent to the negative sequence voltage that causes negative braking torque. Rotating flux opposes the main flux unbalanced voltage operation that will also create a pulsating torque which produces speed pulsation, mechanical vibration and consequently acoustic noise (Gaeid, Ping, Khalid, & Salih, 2011). The resistance fault simulated which occurs in one winding inside the AC motor thereby affecting only one motor phase in a star connected motor. This is indicated in Figure 2. The connecting cable resistance from drive to motor was measured at 0.3Ω for each phase. Therefore, at the maximum fault resistance introduced of 0.4Ω the total resistance between the drive and motor is increased from 0.3Ω to 0.7Ω in the faulty phase leg.

National Electric Motors Association (NEMA) has defined voltage imbalance as (Saleh, 2005):

$$\text{Voltage imbalance} = \left(1 - \frac{3U_{\min}}{\sum U_i}\right) \times 100 \tag{3}$$

where $U_{\min}$ is the lowest phase voltage between three phases, and U_i is the voltage across each phase.

An imbalance in the supply voltage induces sidebands in the stator current spectrum of an induction motor at the following frequencies (Messaoudi & Sbita, 2010).

$$f_{usv} = (1 + 2.k)f_s \tag{4}$$

where the order of harmonics: $k = 1, 2, 3, \ldots,$

Sideband extraction using modulation signal bispectrum (MSB)

The current sideband components can be estimated using spectrum analysis. However, the amplitudes from conventional power spectrum include the additive random noise which is inevitable in measurement systems and motor operating processes and (Chen, Wang, Gu, Haram, & Ball, 2012; Zhang et al., 2017) have shown the consequence of ignoring phase information using power spectrum may degrade diagnosis performance for the case of incipient faults when the sideband amplitude is very small and masked by various random noises: measurement instruments and additional induction currents induced by environment and random magnetic fields. On the other hand, MSB analysis allows the retention of both the amplitude and the phase information, the suppression of random noise and the identification of nonlinear modulation effects.

For a discrete time current or voltage signal $x(t)$ its power spectrum (PS) can be calculated by

$$P(f) = E[X(f)X^*(f)] \tag{5}$$

where $X(f)$ is the discrete Fourier transform:

$$X(f) = \sum_{t=-\infty}^{\infty} x(t)\mathrm{e}^{-2j\pi t} \tag{6}$$

$X^*(f)$ is the complex conjugate of $X(f)$, and $E[\,]$ denotes the statistical expectation. The power spectrum is a linear transform and is a function of the frequency f. Extending this definition by increasing to power of three gives rise to the conventional bispectrum:

$$B(f_1, f_2) = E[X(f_1)X(f_2)X^*(f_1 + f_2)] \tag{7}$$

where, f_1, f_2 and $f_1 + f_2$ indicate the individual frequency components achieved from Fourier series integral.

Bispectrum analysis has a number of unique properties such as nonlinear system identification, phase information retention and Gaussian noise elimination when compared with the power spectrum of Equation (5). Especially, bispectrum is an effective tool for detecting quadratic phase coupling which occurs when two waves interact non-linearly and generate a third wave with a frequency and phase equal to the sum or difference of

the first two waves. This also means that it is particularly useful to characterize harmonics components which commonly presents in vibro-acoustic signals.

Conventional bispectrum of Equation (7) characterize only the presence of quadratic phase coupling (QPC) from the harmonically related frequency components of f_1, f_2 and $f_1 + f_2$. It neglects the possibility that the occurrence of $f_1 - f_2$, the lower sideband in PS may be also due to the nonlinear relationship between the two components of f_1 and f_2. Because of this, it is not adequate to describe amplitude modulation (AM and FM) signals such as motor current signals (Gu et al., 2015).

To improve the performance of the conventional bispectrum in characterizing the motor current signals, a new variant of the conventional bispectrum, named as a modulation signal bispectrum (MSB) is examined (Alwodai, Yuan, et al., 2012; Gu et al., 2011, 2015) as in Equation (8):

$$B_{\mathrm{MS}}(f_1,\ f_2) = E[X(f_2 + f_1)X(f_2 - f_1)X^*(f_2)X^*(f_2)] \quad (8)$$

The total phase of MSB

$$\varphi_{\mathrm{MS}}(f_1,\ f_2) = \varphi(f_2 + f_1) + \varphi(f_2 - f_1) - \varphi(f_2) - \varphi(f_2) \quad (9)$$

When two components f_1 and f_2 are coupled, their phases are related by

$$\begin{aligned} \varphi(f_2 + f_1) &= \varphi(f_2) + \varphi(f_1) \\ \varphi(f_2 - f_1) &= \varphi(f_2) - \varphi(f_1) \end{aligned} \quad (10)$$

By substituting Equation (10) into Equation (9) the total phase of MSB will be zero and MSB amplitude will be the product of the four magnitudes, which is the maximum of the complex product. Therefore, a bispectral peak will appear at $(f_1,\ f_2)$. Equation (8) now takes into account both $(f_1 + f_2)$ and $(f_1 - f_2)$ for systematically measuring the nonlinearity of modulation signals. If $(f_1 + f_2)$ and $(f_1 - f_2)$ are both due to nonlinear effect between f_1 and f_2 a bispectral peak will appear at bifrequency $B_{\mathrm{MS}}(f_1,\ f_2)$. This is more accurate and efficient in representing the sideband characteristics of modulation signals.

Because a motor current signal with electrical and mechanical faults contains a series of sideband components which appear mainly around the supply component, a bispectrum slice at the supply frequency will be sufficient to characterize these sidebands for fault detection and diagnosis. By setting f_2 in Equation (8) into a constant frequency value such as the fundamental $f_2 = f_s =$ 50 Hz, an MSB slice at supply frequency can be expressed as:

$$B_{\mathrm{MS}}(f_1,\ f_s) = E[X(f_s + f_1)X(f_s - f_1)X^*(f_s)X^*(f_s)] \quad (11)$$

The amplitude of supply frequency is predominant in current signals and it can be identified easily in the frequency domain, an MSB slice based sideband estimator, abbreviated as MSB-SE, can be introduced as:

$$\begin{aligned} B^{\mathrm{SE}}_{\mathrm{MS}}(f_1,\ f_s) = E[&X(f_s + f_1)X(f_s - f_1)X^*(f_s)/|X(f_s)| \\ &\times X^*(f_s)/|X(f_s)|] \end{aligned} \quad (12)$$

MSB-SE can also have its coherence function. According to (Gu et al., 2011) and Equation (12), MSB-SE coherence can be obtained by

$$b^2{}_{\mathrm{MSB-SE}}(f_1,\ f_s) = \frac{|B^{\mathrm{SE}}_{\mathrm{MS}}(f_1,\ f_s)^2|}{E[|X(f_s + f_1)X(f_s - f_1)|^2]} \quad (13)$$

To confirm the coupling effects between sidebands and carrier and to check the degree of random noise influence, which allows confirmation of the existence of MSB-SE peaks for the detection of modulation process in noise measurements.

Effect of the fault on the VSD fed motors

An inverter-driven motor system controls the rotational speed of an alternating current (AC) electric motor by controlling the frequency and voltage of the electrical power supplied to the motor. The speed of an Alternating Current (AC) motor depends on three principle variables (Lane, 2011; Saad, 2015):

- The pole number which determines the motor's base speed
- The frequency of the AC line voltage

Variable speed drives change this frequency to change the speed of the motor.

- The amount of torque loading on the motor which causes slip

Therefore when continuous adjustable speed over a wide range is desired, the best method is to provide a variable frequency supply (Saad, 2015). This is carried out by means of variable frequency drive (VFD). This system is also called an inverter, adjustable-frequency drive (AFD), adjustable speed drives (ASD) and variable speed drive (VSD). Various types of AC induction motors and variable speed drive systems are available for different applications and diverse methodologies are used for monitoring their conditions. However, this paper mainly focuses on the Sensorless Flux Vector Control for AC three phase induction motors.

The sensorless drive is considered as it is very commonly used in industries. However, closed loop and

field oriented control, either with speed feedback sensors or sensorless, are all based on feedback regulation and electrical faults can have nearly the same effect on them (Ong, 1998). Sensorless field orientated control (FOC) drives control the IMs speed without any speed feedback devices. Motor model and parameters together with supply measurements are utilized to control the *d-q* axis electrical supply quantities. Sensorless FOC drives provide (Hughes & Drury, 2013; Lane, Ashari, Ball, & Gu, 2015; Saad, 2015).

- Automatic slip compensation
- High motor torque at low output frequencies
- Improved dynamic response to demand and load variations
- Compactness with less maintenance
- Simpler application with no need for wires
- Avoidance of the cost of encoders
- Suitability for different environments, including temperature.

In this drive mode, a feedback loop is used for providing better speed regulation and enhanced dynamic response and the drive used is sensorless variable speed drive based on Model Reference Adaptive System (MRAS). The output voltage is separately regulated utilizing the knowledge of phase angle, while the frequency is controlled by switching the time of the inverter (Ong, 1998; Shaeboub, Abusaad, Hu, Gu, & Ball, 2015). Model Reference Adaptive System (MRAS) is one of the most frequently used schemes in industrial applications (Saad, 2015). It is also represented here as it is used in the test rig drive upon which this study is based. MRAS utilizes two independent machine models for estimating the same state variable, namely reference and adaptive model (Hiremath & Kaur, 2015). The error between two models estimates induction motor speed. The model that does not involve the quantity to be estimated is considered as the reference model. The model that has the quantity to be estimated involved is considered as the adaptive model. Comparison between the two models outputs generates an error signal that is treated by an adaptation mechanism (Hiremath & Kaur, 2015). Model reference adaptive system speed estimator based on voltage (reference model) and current (adjustable or adaptive) model represents in Figure 3.

The reference model is composed of the stator voltage equations as follows (Saad, 2015; Zerdali & Barut, 2013).

$$\frac{\mathrm{d}\psi^{u}\alpha r}{\mathrm{d}t} = \frac{L_{\mathrm{r}}}{L_{\mathrm{m}}}\left(u_{\alpha \mathrm{s}} - R_{\mathrm{s}} i_{\alpha \mathrm{s}} - \sigma L_{\mathrm{s}} \frac{\mathrm{d}i_{\alpha \mathrm{s}}}{\mathrm{d}t}\right) \tag{14}$$

$$\frac{\mathrm{d}\psi^{u}\beta r}{\mathrm{d}t} = \frac{L_{\mathrm{r}}}{L_{\mathrm{m}}}\left(u_{\beta \mathrm{s}} - R_{\mathrm{s}} i_{\beta \mathrm{s}} - \sigma L_{\mathrm{s}} \frac{\mathrm{d}i_{\beta \mathrm{s}}}{\mathrm{d}t}\right) \tag{15}$$

The adjustable (adaptive) model is represented as follows (Saad, 2015; Zerdali & Barut, 2013):

$$\frac{\mathrm{d}\psi^{i}\alpha r}{\mathrm{d}t} = \frac{1}{T_{\mathrm{r}}}(L_{\mathrm{m}} i_{\alpha \mathrm{s}} - \psi^{i}\alpha r - T_{\mathrm{r}}\hat{\omega}_{\mathrm{r}}\psi^{i}\beta r) \tag{16}$$

$$\frac{d\psi^{i}\beta r}{dt} = \frac{1}{T_{r}}(L_{m} i_{\beta s} - \psi^{i}\beta r + T_{r}\hat{\omega}_{r}\psi^{i}\alpha r) \tag{17}$$

$$\sigma = 1 - \frac{L^{2}m}{L_{\mathrm{r}}L_{\mathrm{s}}} \tag{18}$$

where, L_{ls}, L_{lr} are the per phase winding leakage inductances in the stator and rotor, respectively, L_{m} is the motor mutual inductance, L_{s}, L_{r} are stator and rotor inductances, ψ_{r},ψ_{s} are rotor and stator flux, σ is motor leakage coefficient, T_{r} is rotor time constant and Subscripts α and β Represent the stationary reference frame coordinates.

The error between the two models is calculated in the following way (Saad, 2015):

$$e = \psi^{u}{}_{\beta r}\psi^{i}{}_{\alpha r} - \psi^{u}{}_{\alpha r}\psi^{i}{}_{\beta r} \tag{19}$$

The most common method used for the adaptation mechanism is the PI controller, although certain other

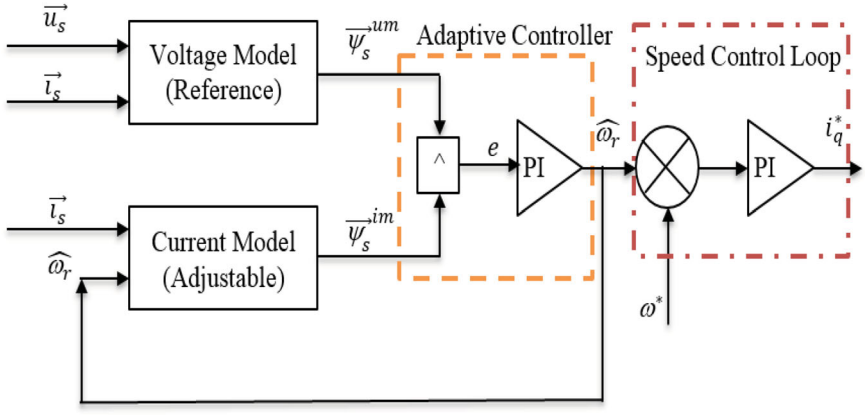

Figure 3. Schematic of MRAS and speed loop in a Sensorless drive (Saad, 2015).

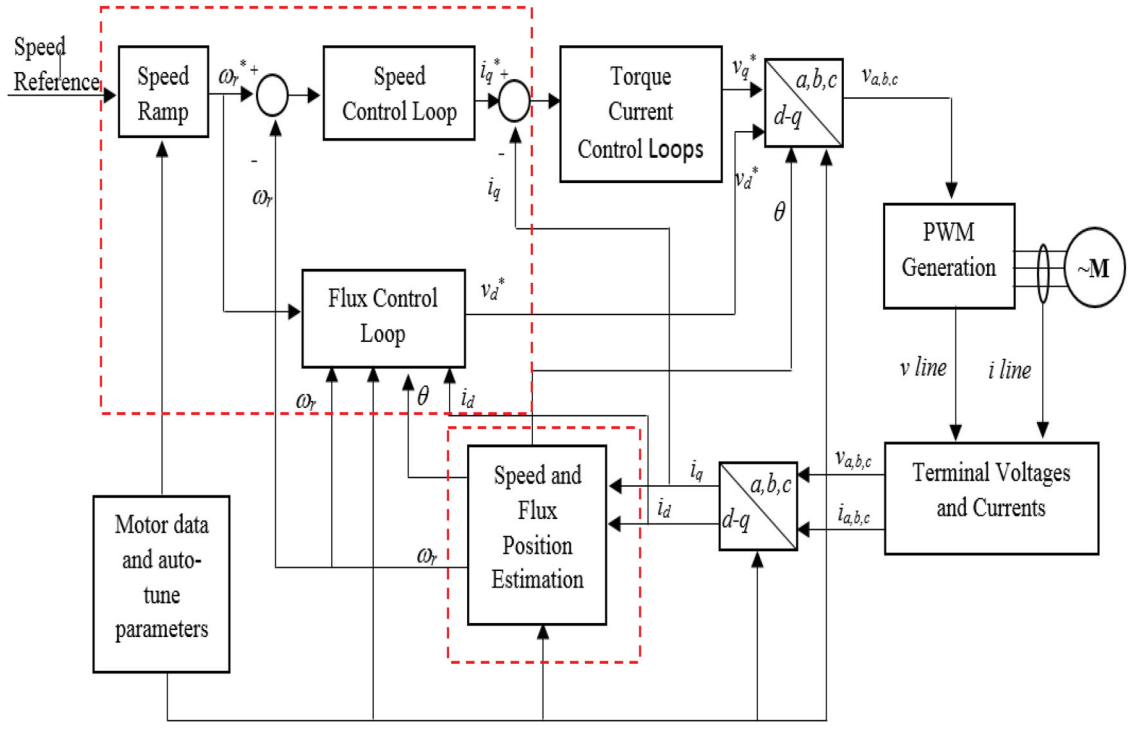

Figure 4. A block diagram of a general FOC drive (Saad, 2015).

techniques are used such as fuzzy and neural network control systems (Luo, Wang, Wei, & Alsaadi, 2017). The output from the PI controller replaces the estimated value in the adjustable model. The MRAS continually modifies the estimated variable quantity maintaining the error between the two models (Ahmed, 2015; Saad, 2015). The estimated speed is then used to calculate the rotor flux angle θ_e as follows:

$$\theta_e = \int \omega_e dt \tag{20}$$

The estimated speed from MRAS is fed into the speed loop for speed control as illustrated in Figure 3. The outer is a speed PI control loop which compares the reference speed with the feedback speed and generates the speed error. The speed error sets the reference value of the inner control loops. The inner control loops are two PI control loops in series, i.e. the current control loop that sets the reference torque signal based on the difference between the actual current and the reference from the speed loop; and the torque control loop that sets the reference value for the voltage output based on the difference between the feedback torque and reference from the current loop. The fourth is the voltage control loop that gives the control action to the PWM to feed the motor with the required voltages and frequencies.

A block diagram of a general sensorless flux vector control drive can be shown in Figure 4. The torque reference will include as frequency components which will be directed to the voltage regulators as an output voltage to the motor supply.

It is also worth mentioning that when a fault occurring in the motor is not big enough, the drive regulator actions, together with the noise from the PWM switches masks such fault features in the current signal and make detection more difficult (ABB, 1996). In the meantime, the regulations also propagate the fault characteristics into the voltages, therefore, in closed loop systems the voltage signals are likely to be more sensitive to stator and rotor faults than the current signals.

Test facility

To evaluate the analysis in the previous section, an experimental study was conducted based on a three-phase induction motor with rated output power of 4 kW at speed 1420 rpm (two-pole pairs), as shown in Figure 5. A digital variable speed drive operating with a sensorless closed loop is employed to control the motor speed. The induction motor is coupled to a loading DC generator using a flexible spider coupling. The DC load generator is controlled by a DC variable drive that varies the armature current in the DC load generator to provide the required load to the AC motor. The operating speeds and loads are set by the operator via a touch screen on the control panel.

To investigate the characteristics of the current and voltage signals, a power supply measurement device

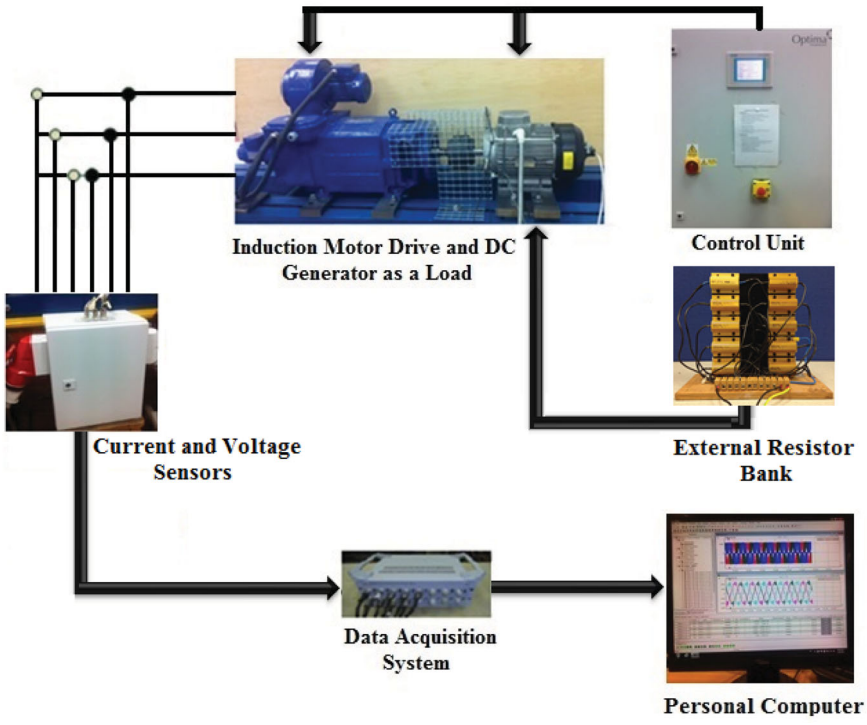

Figure 5. A photograph of the test rig facility.

was employed to measure the AC voltages, currents and power using Hall Effect voltage and current transducers and a universal power cell, which is independent of the controller to avoid any interruptions to the control process. During the experimental work all the data was recorded using a YE6232B high speed data acquisition system. This system has 16 channels, each channel with a 24 bit analogue-digital converter at a sampling frequency of 96 kHz. The three phase currents, voltages and encoder pulse trains (for speed measurements) were acquired simultaneously under steady operations. The data for each operation was recorded for 30 s to allow for 100 averages in MSB and PS calculation and obtain reliable results.

In order to evaluate the performance of MSB analysis, current and voltage signals were collected for five diverse motor formations: healthy motor (BL), one broken rotor bar (1BRB), two broken rotor bar (2BRB) which are depicted in Figure 6. They were induced by drilling carefully into the bars along their height in such a way that the hole cut the bar completely to simulate the broken rotor bar fault. Subsequently, the tests were further carried out when the 1BRB is compounded with a phase winding resistance increment ($R_{fs} = 0.4\Omega$) and 2BRB with ($R_{fs} = 0.4\Omega$), in which the resistance increments were realized by an external resistor bank connected into one of the three winding phases, as shown in Figure 5.

In all test cases, the motor ran under five successive load increments: 0%, 20%, 40%, 60%, and 80% of full load,

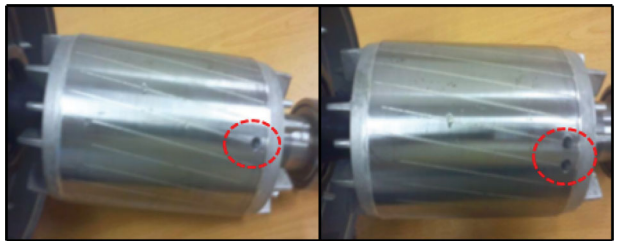

Figure 6. Rotor with one and two broken bars.

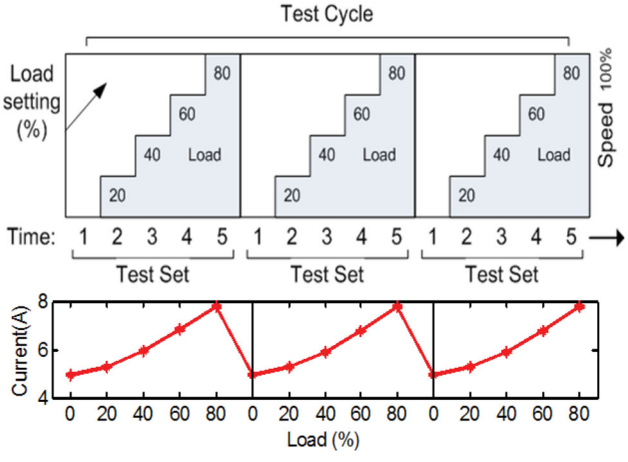

Figure 7. Load cycle for three repeat tests.

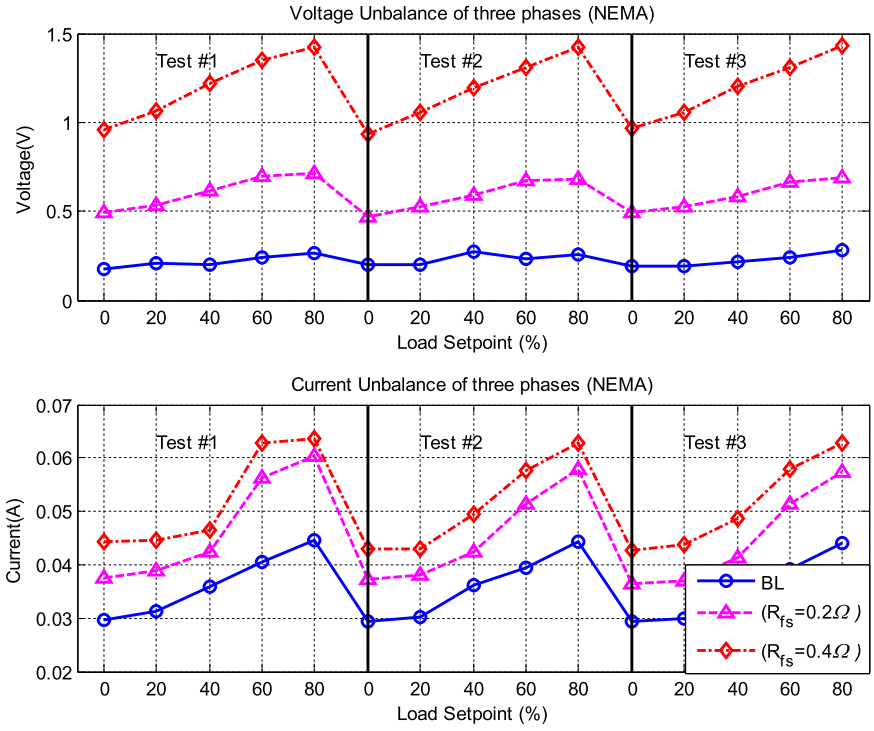

Figure 8. Voltage and current imbalances by NEMA definitions.

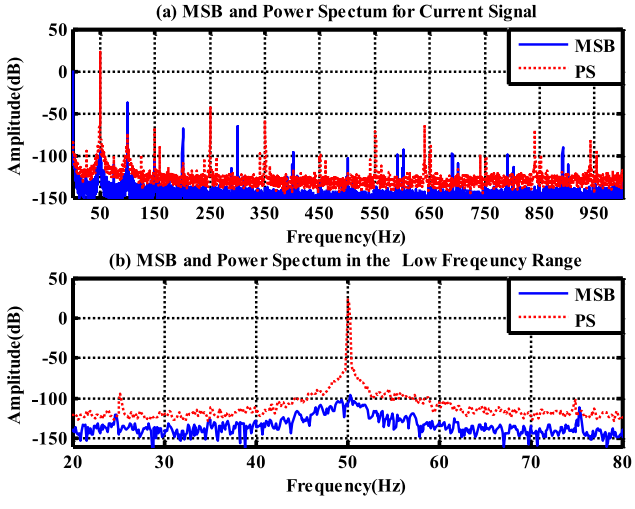

Figure 9. MSB and power spectrum characteristics for current signals.

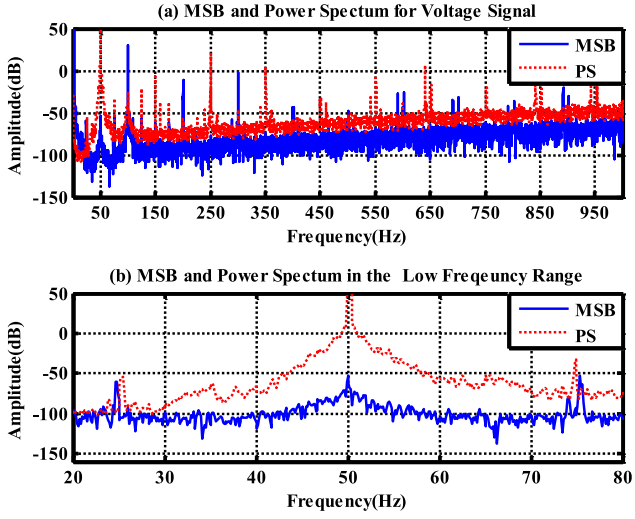

Figure 10. MSB and power spectrum characteristics for voltage signals.

which lets the investigative performance to be inspected at variable loads and avoid any probable damages of the test system when faults are simulated at the full load. As shown in Figure 7, each of the five loading increments has been repeated three times, making a total of 15 load steps. An example plot is shown in Figure 7. This test step diagram also indicates how the test results are presented. Where vertical lines are shown in any plot, these represent the start of each new load test cycle.

Results and discussion

Broken rotor bar with phase winding resistance increments ($R_{fs} = 0.4\Omega$)

The current and voltage readings show that there is a noticeable difference in current and voltage imbalances when the fault resistance is introduced. The maximum is 1.068 V at 80% loading for the 0.4Ω fault resistance. Figure 8 indicates the results of calculating motor voltage

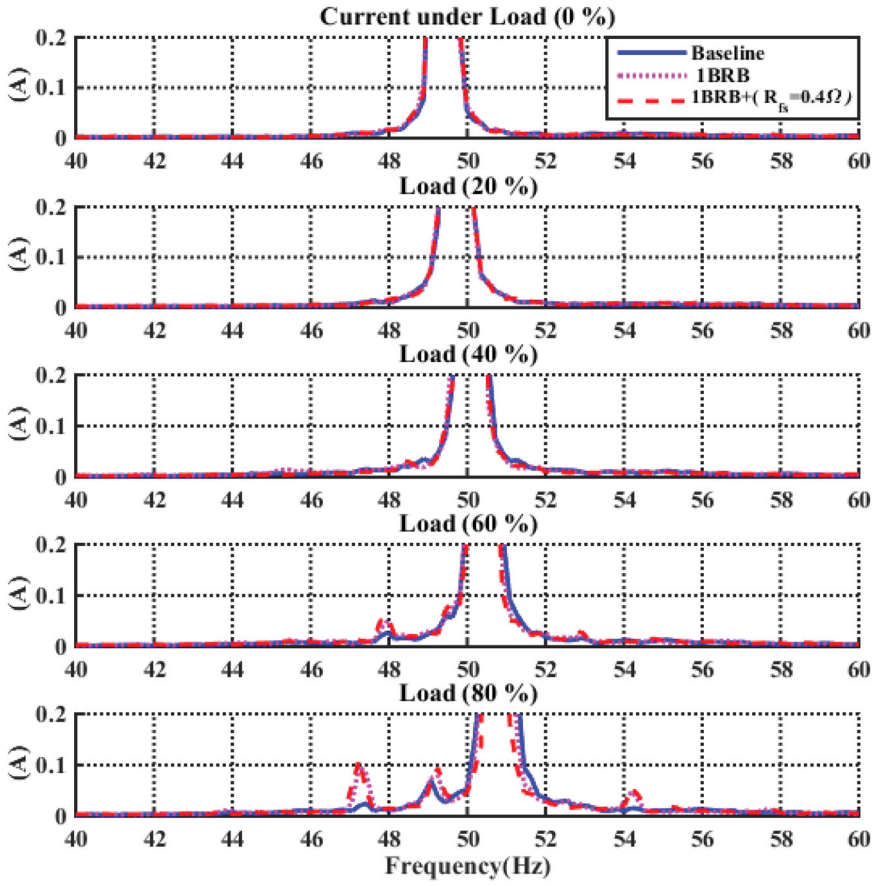

Figure 11. Phase current spectra for BL, 1BRB, 1BRB with $R_{fs} = 0.4\Omega$ under different loads.

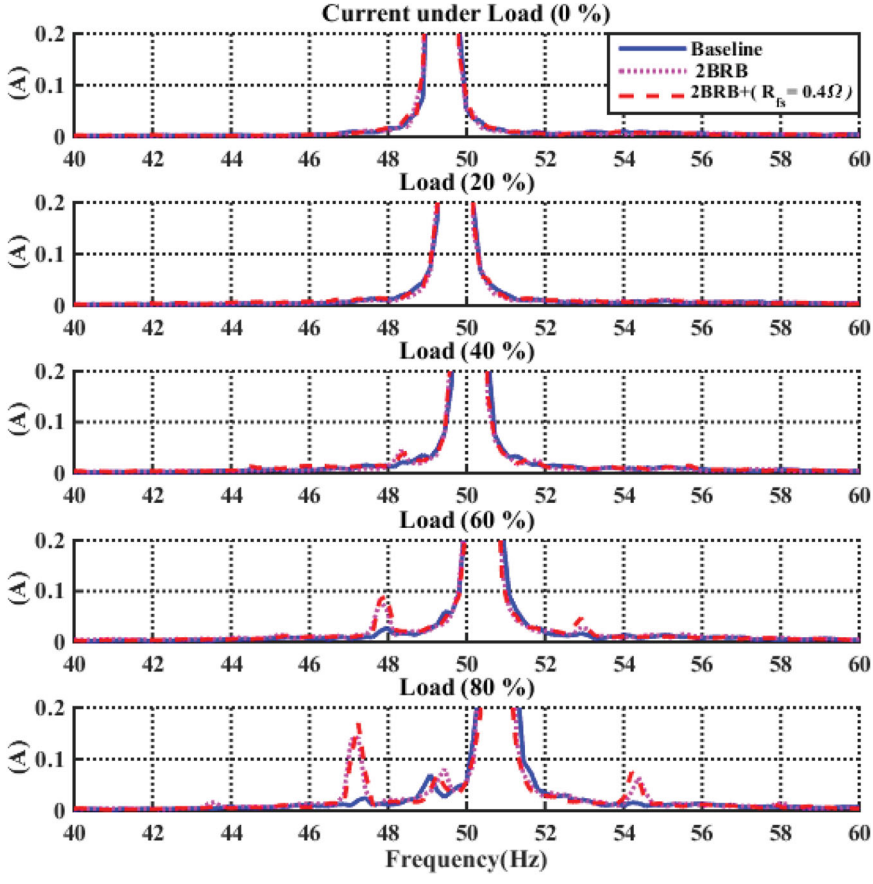

Figure 12. Phase current spectra for BL,2BRB, 2BRB with $R_{fs} = 0.4\Omega$ under different loads.

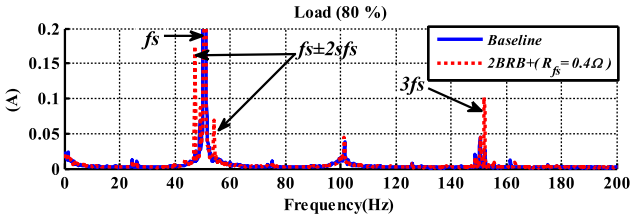

Figure 13. Phase current spectra for baseline, and 2BRB with $R_{fs} = 0.4\Omega$.

and current imbalances across all phases in accordance with the NEMA definition.

Figures 9 and 10 show a direct comparison between a modulation signal bispectrum slice at the supply frequency and power spectrum for the current and voltage signals under 40% load at full speed when the motor is baseline (healthy). MSB shows very good performance in noise reduction, comparing it with power spectrum as shown in Figure 9 (a) and Figure 10 (a). The 50 Hz supply component in the power spectrum is eliminated completely in the modulation signal bispectrum. This makes it easier and more reliable to observe components that relate to motor health conditions. The sideband components $(f_s - f_r)$ and $(f_s + f_r)$ around f_s shown by power spectrum of Figure 9 (b) and Figure 10 (b) is now represented by a single component at 24.88 Hz in modulation signal bispectrum. This makes spectral peaks such as that due to stator faults in the high frequency range to be estimated more accurate and thus better diagnostic results.

Figures 11 and 12 show the spectrum of stator current under healthy (BL) and the faulty cases at full speed and under loads 0%, 20%, 40%, 60% and 80% with respect to 0.4Ω winding asymmetry. It can be seen that there are no visible sidebands for one broken rotor bar and combined fault under 0% and 20% motor load since the slip is too small to be identified as shown in Figure 11.

However, clear sidebands are available for the same broken rotor bar fault under 40% motor load and when the motor load is increased to 80% load, the amplitude of sidebands increase. However, not much of a difference can be seen in the Figure 11 when the load touches 80% and the maximum amplitude of the current are significantly increased by increasing the resistor imbalance factor.

It is also clear that the amplitude of side band increases as the severity of the fault and load increases as shown in Figure 12 and the fault can be best detected under higher load.

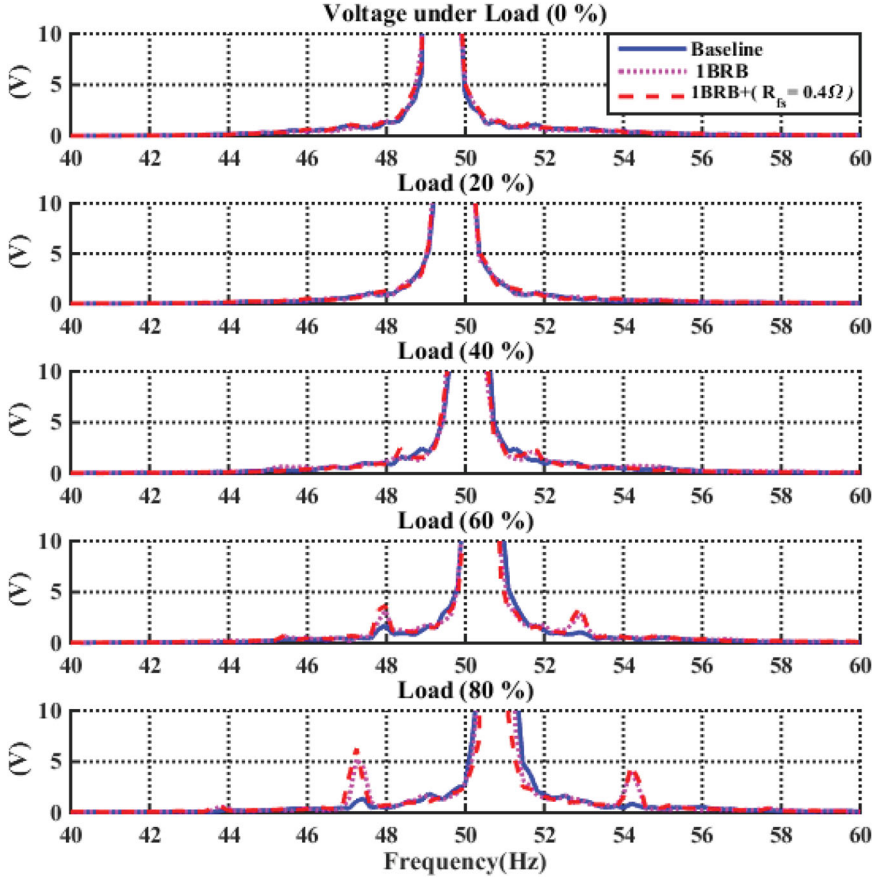

Figure 14. Voltage spectra for BL, 1BRB, 1BRB with $R_{fs} = 0.4\Omega$ under different loads.

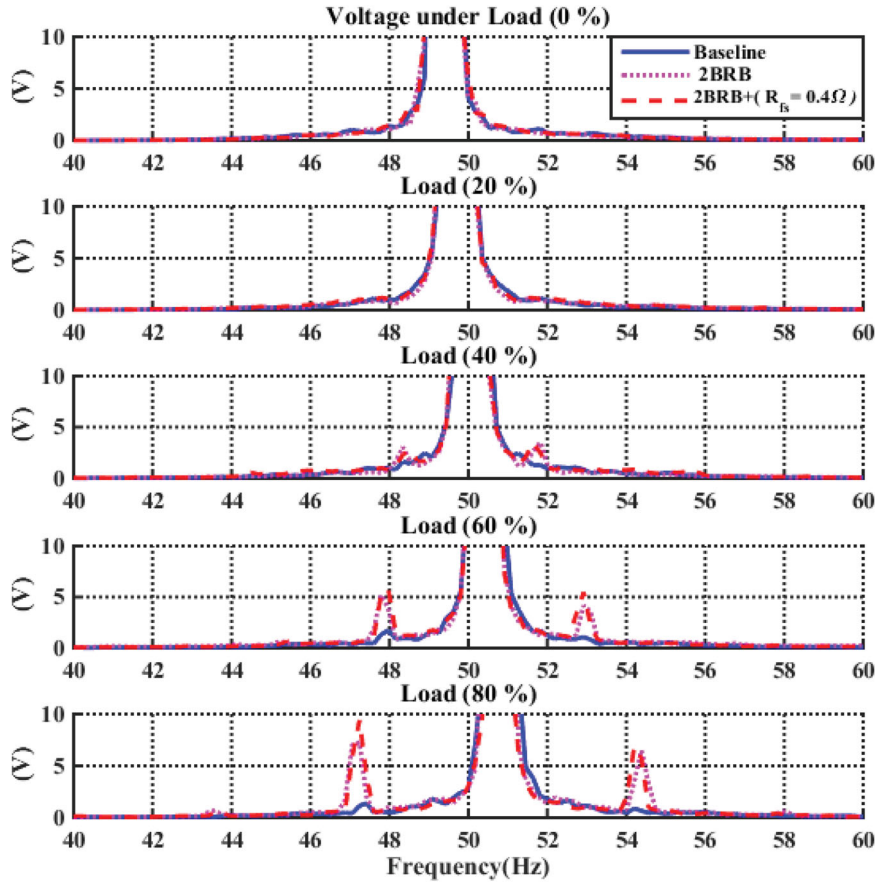

Figure 15. Voltage spectra for BL, 2BRB, 2BRB with $R_{fs} = 0.4\Omega$ under different loads.

Figure 13 clarifies that the additional increase of the sidebands at $f_s(1 \pm 2ks)$ is due to the stator winding asymmetry that has an amplitude increase at $3fs$.

Figures 14 and 15 depict the output voltage spectra from the drive to the motor terminals. The sidebands of voltage increase in amplitude with load and severity of the fault. The main concern of this domain is that how effective motor voltage signature analysis (MVSA) is when it comes to analysing and detecting faults that occur in an induction motor. The sensorless control mode gives measurable indication of the fault as soon as load reaches 40%, and at 80% load the graph shows prominent increases in sidebands and the results show some notable and inevitable changes as shown in Figure 15. This proves that sensorless control mode allows more accurate and efficient outputs.

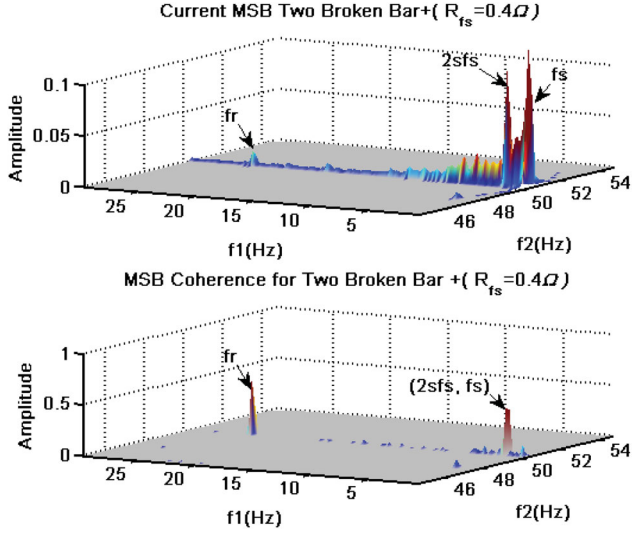

Figure 16. Characteristics of current MSB for 2BRB with asymmetry resistance 0.4Ω under 60% load.

Characteristics of MSB

Figure 16 presents typical MSB results (MSB magnitude and MSB coherence) from the current signal under two broken bars with a phase winding resistance increment ($R_{fs} = 0.4\Omega$) and 60% load with respect to sensorless control mode. As it can be seen in Figure 16, MSB shows two distinctive peaks at bifrequency (2.56, 50.0) Hz and (24.54, 50.0) Hz in the bifrequency domain. Clearly, the first one relates to the *2sfs* and can be relied on to detect and diagnose BRB without doubt, whereas the second one relates

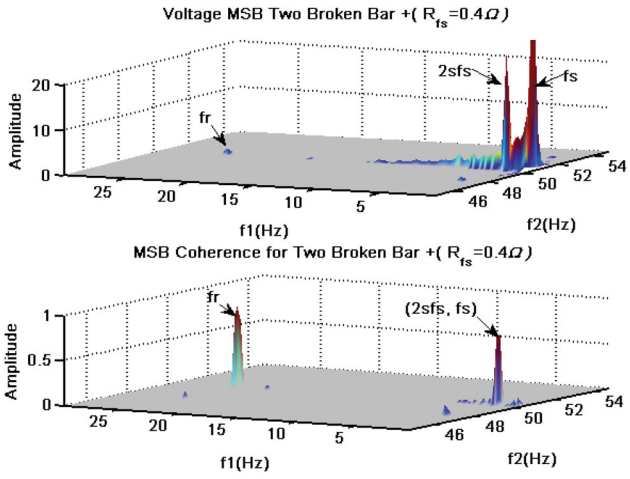

Figure 17. Characteristics of voltage MSB for 2BRB with asymmetry resistance 0.4Ω under 60% load.

to rotor speed due to the speed oscillation. Moreover, these two peaks are also distinctive in MSB coherence, confirming that they stem from modulation processes between $2sf_s$ and f_s, and f_r and f_s respectively, and that these modulations have good signal to noise ratio which can be relied on to ensure the results.

Figure 17 presents MSB results from the voltage signal under the same conditions as Figure 16. Similarly, the two distinctive peaks at bifrequency (2.56, 50.0) Hz and (24.54, 50.0) Hz can be used to diagnose the BRB and the winding asymmetry respectively, showing that the voltage signals also have the faulty information.

Moreover, comparing the MSB coherences between the current and voltage signals, it can be seen that the coherence amplitudes of the voltage signals are clearly higher (larger than 0.5) than that of the current signals. This means that the voltage signal has a higher signal to noise ratio with respect to the two fault components. Therefore, in closed loop systems the MSB based on voltage signals is more sensitive to these faults and hence produces more accurate results than current signals. This can be explained that the VSD regulates the voltage to adapt changes in the electromagnetic torque caused by these faults.

Comparison between techniques

A comparative study of different condition monitoring techniques which include modulation signal bispectrum and power spectrum based on current and voltage signals has taken into consideration both healthy and combined fault conditions. Figure 18 shows the diagnostic performance comparison of current signals under different fault cases and different loads with respect to

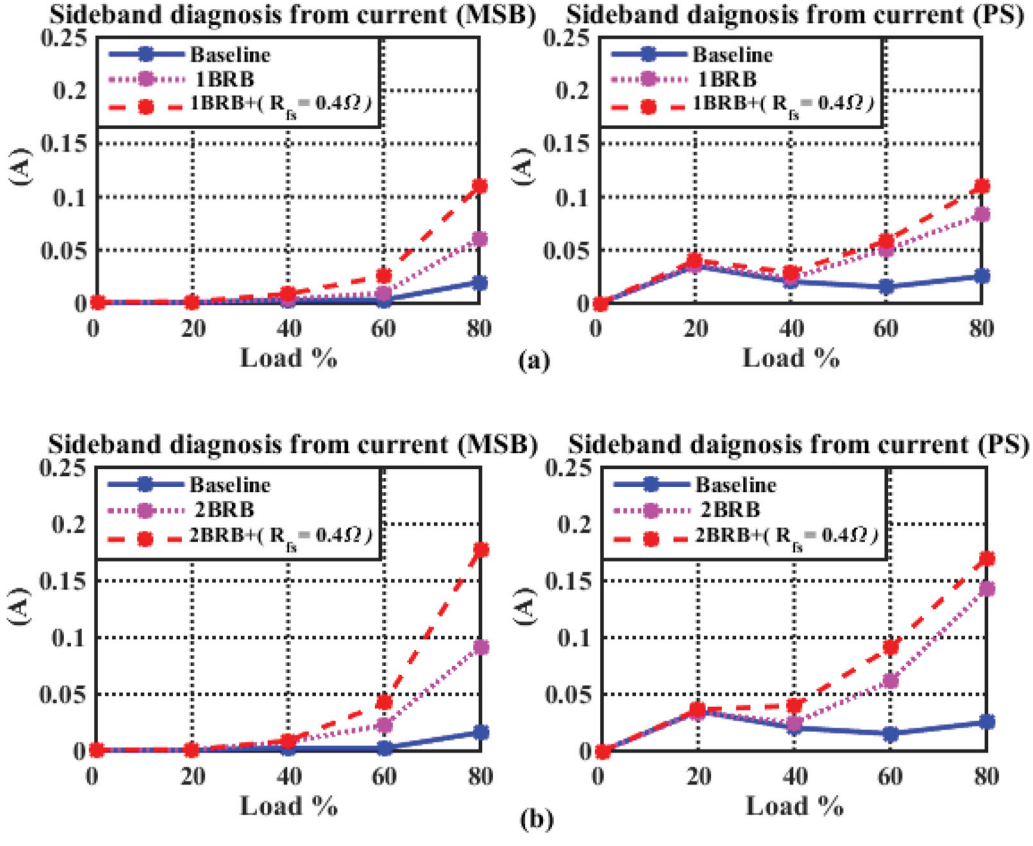

Figure 18. Current signal based diagnosis comparison between MSB and PS.

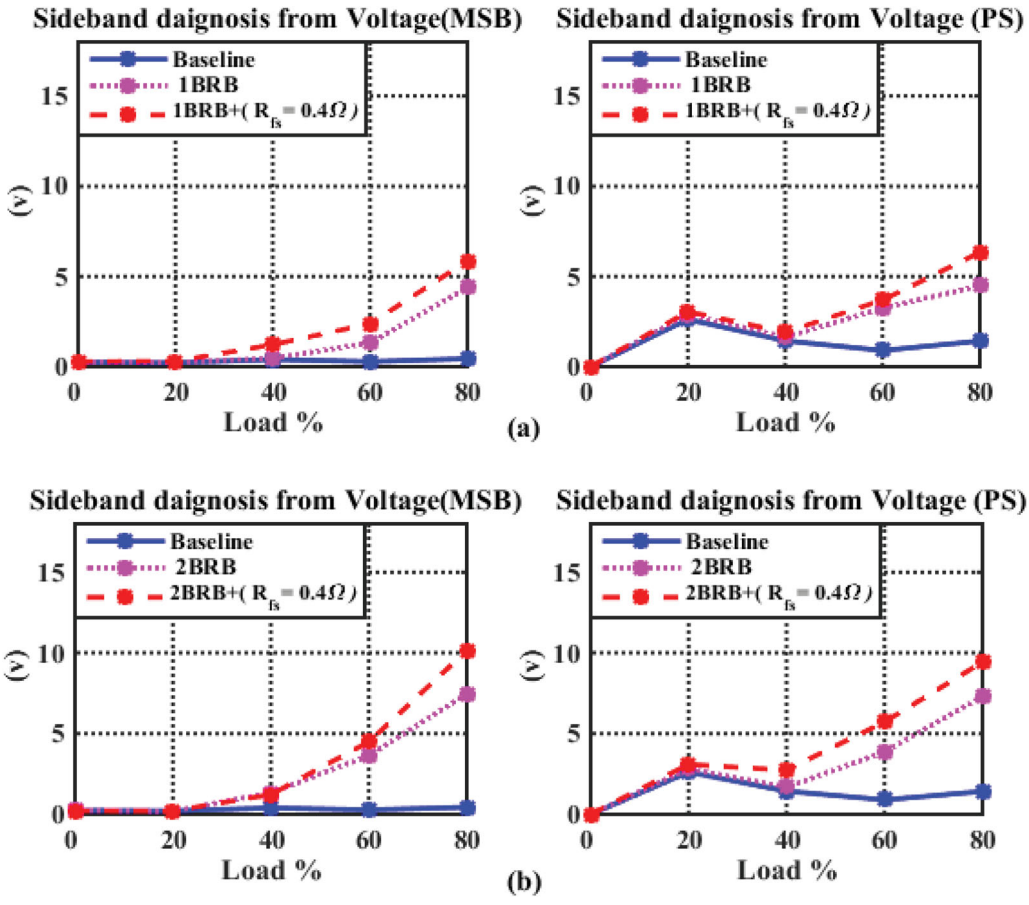

Figure 19. Voltage signals based diagnosis comparison between MSB and PS.

the sensorless control mode in which the performance parameters are the peak magnitudes extracted from two spectrum analysis at $2sf_s$. It is significant that the amplitude of sideband increases as the severity of the fault and load increase, and both PS and MSB peaks allow the faults to be detected under higher loads (60% and 80% of the full loads). However, MSB gives gradual and hence better severity separations due to its high performance in noise reduction. Moreover, MSB also avoid incorrect diagnosis under the lower load conditions (20% loads) where PS may provide an inadequate diagnosis due to its significant values, even for the healthy conditions.

Similar to the current signal based diagnosis shown in Figure 18, the voltage based diagnosis shown in Figure 19 is also able to provide further support that MSB provides better diagnostic performances in that it separates the fault severity better under high loads and avoids misdetection under lower loads. In addition, the MSB diagnosis based voltage signals can show more sensitive detection at the lower load of 40% as its peak values are clearly higher than the baseline, compared with that of current signals.

In general, this experimental evaluation shows that the MSB based diagnosis performs better than the PS one and the voltage signals give slightly better results than the current signals.

Conclusion

This paper has shown the effectiveness of using both motor current and voltage signals for detection and diagnosis of motors faults compound between rotors and stators under sensorless control mode. The results show that the additional increase of the sidebands at $2sf_s$ is due to the stator winding asymmetry that has an amplitude increase at $3f_s$ and this increase in sidebands can be observed in both the current and voltage signals. In a power spectrum they exhibit as asymmetric sidebands around the supply frequency. These sidebands can be quantified more accurately using a new MSB-SE estimator, which results in more consistent detection and accurate diagnosis of the fault severity. Additionally, MSB coherence results have also confirmed that voltage signals under sensorless control mode have a higher signal to noise ratio with respect to the faults.

Acknowledgement

The authors thank the Natural and Scientific foundation of China, (NO. 51375326), who supported this paper.

Disclosure statement

No potential conflict of interest was reported by the authors.

References

ABB. (1996). *High performance drives speed and torque regulation* [Technical Guide No. 100]. ABB Industrial Systems. Retrieved from https://library.e.abb.com/public/8492cb383e941d57852571c3006b0194/Speedtorq.pdf

Ahmed, A. H. O. (2015). Speed sensorless vector control of induction motors using rotor flux based model reference adaptive system. *Journal of Engineering and Computer Science (JECS)*, *16*(3), 1–4.

Alwodai, A., Gu, F., & Ball, A. (2012). A comparison of different techniques for induction motor rotor fault diagnosis. *Journal of Physics: Conference Series*, *364*(1), article no. 012066. doi:10.1088/1742-6596/364/1/012066

Alwodai, A., Yuan, X., Shao, Y., Gu, F., & Ball, A. (2012). *Modulation signal bispectrum analysis of motor current signals for stator fault diagnosis*. 18th International Conference on Automation and Computing (ICAC), Loughborough, UK. IEEE.

Alwodai, A. M. M. (2015). *Motor fault diagnosis using higher order statistical analysis of motor power supply parameters* (PhD). University of Huddersfield.

Ashari, D., Lane, M., Gu, F., & Ball, A. (2014). *Detection and diagnosis of broken rotor bar based on the analysis of signals from a variable speed drive*. 3rd International Workshop and Congress on eMaintenance, Lulea, Sweden, June 17–18, 2014.

Ceban, A., Pusca, R., Romary, R., & Lecointe, J.-P. (2011). Diagnosis of inter-turn short circuit fault in induction machine. *Annals of the University of Craiova, Electrical Engineering Series*, *35*, 103–110.

Chen, Z., Wang, T., Gu, F., Haram, M., & Ball, A. (2012). Gear transmission fault diagnosis based on the bispectrum analysis of induction motor current signatures. *Journal of Mechanical Engineering*, *48*(21), 84–90.

Constantine, R. A. E. (2014). *Effects of mixed faults on the stator current spectrum of the induction machine*. WSEAS, Conference/ ELECT-06, Istanbul.

El Hachemi Benbouzid, M. (2000). A review of induction motors signature analysis as a medium for faults detection. *IEEE Transactions on Industrial Electronics*, *47*(5), 984–993.

Gaeid, K. S., Ping, H. W., Khalid, M., & Salih, A. L. (2011). Fault diagnosis of induction motor using MCSA and FFT. *Electrical and Electronic Engineering*, *1*(2), 85–92.

Garcia-Perez, A., de Jesus Romero-Troncoso, R., Cabal-Yepez, E., & Osornio-Rios, R. A. (2011). The application of high-resolution spectral analysis for identifying multiple combined faults in induction motors. *IEEE Transactions on Industrial Electronics*, *58*(5), 2002–2010.

Gu, F., Shao, Y., Hu, N., Naid, A., & Ball, A. (2011). Electrical motor current signal analysis using a modified bispectrum for fault diagnosis of downstream mechanical equipment. *Mechanical Systems and Signal Processing*, *25*(1), 360–372.

Gu, F., Wang, T., Alwodai, A., Tian, X., Shao, Y., & Ball, A. (2015). A new method of accurate broken rotor bar diagnosis based on modulation signal bispectrum analysis of motor current signals. *Mechanical Systems and Signal Processing*, *50–51*, 400–413.

Hiremath, C., & Kaur, P. (2015). Implementation of sensorless vector control technique based on MRAS speed estimator for parallel connected induction motors. *International Journal of Scientific Research and Education*, *3*(6), 3704–3713.

Hughes, A., & Drury, B. (2013). *Electric motors and drives: Fundamentals, types and applications* (4th ed.). Oxford: Newnes.

Hussein, N. A., Mahmood, D. Y., & Abdulbaqi, I. M. (2011). 3-phase induction motor bearing fault detection and isolation using MCSA technique based on neural network algorithm. *International Journal Applications Engineering Researcher*, *5*(6), 581–591.

Kersting, W. (2001). Causes and effects of unbalanced voltages serving an induction motor. *IEEE Transactions on Industry Applications*, *37*(1), 165–170.

Lamim Filho, P., Pederiva, R., & Brito, J. (2014). Detection of stator winding faults in induction machines using flux and vibration analysis. *Mechanical Systems and Signal Processing*, *42*(1), 377–387.

Lane, M. (2011). *Using the AC drive motor as a transducer for detecting electrical and electromechanical faults* (Masters thesis). University of Huddersfield.

Lane, M., Ashari, D., Ball, A., & Gu, F. (2015). *Investigation of motor supply signature analysis to detect motor resistance imbalances*. Proceedings of the 21st International Conference on Automation and Computing (ICAC). IEEE.

Luo, Y., Wang, Z., Wei, G., & Alsaadi, F. E. (2017). Robust $\mathscr{H}_\infty$ filtering for a class of Two-dimensional uncertain fuzzy systems With randomly occurring mixed delays. *IEEE Transactions on Fuzzy Systems*, *25*(1), 70–83.

Messaoudi, M., & Sbita, L. (2010). Multiple faults diagnosis in induction motor using the MCSA method. *International Journal of Signalling and Image Processing*, *1*(3), 190–195.

Mirabbasi, D., Seifossadat, G., & Heidari, M. (2009). *Effect of unbalanced voltage on operation of induction motors and its detection*. 2009 International Conference on Electrical and Electronics Engineering - ELECO 2009, Bursa, Turkey, IEEE.

Ong, C.-M. (1998). *Dynamic simulation of electric machinery: Using MATLAB/SIMULINK*. Upper Saddle River, NJ: Prentice Hall PTR.

Payne, B. S. (2003). *Condition monitoring of electrical motors For improved asset management* (PhD). University of Manchester.

Saad, S. A. A. (2015). *The utilisation of information avalable in the sensorless control system of an AC induction motor for condition monitoring* (PhD). University of Huddersfield.

Sahraoui, M., Zouzou, S., Ghoggal, A., & Guedidi, S. (2010). *A new method to detect inter-turn short-circuit in induction motors*. The XIX International Conference on Electrical Machines - ICEM 2010, Rome, Italy. IEEE.

Saleh, A. F. (2005). *Detection and diagnosis of electrical faults In induction motors using instantaneous phase variation* (PhD). University of Manchester.

Shaeboub, A., Abusaad, S., Hu, N., Gu, F., & Ball, A. D. (2015). *Detection and diagnosis of motor stator faults using electric signals from variable speed drives*. 21st International Conference on Automation and Computing (ICAC), Glasgow, UK. IEEE.

Sharifi, R., & Ebrahimi, M. (2011). Detection of stator winding faults in induction motors using three-phase current monitoring. *ISA Transactions*, *50*(1), 14–20.

Sridhar, S., & Rao, K. U. (2013). *Detection of simultaneous unbalanced under-voltage and broken rotor fault in induction motor*. 1st international conference on Condition Assessment Techniques in Electrical Systems (CATCON), Kolkata, India. IEEE.

Vamvakari, A., Kandianis, A., Kladas, A., Manias, S., & Tegopoulos, J. (2001). Analysis of supply voltage distortion effects on induction motor operation. *IEEE Transactions on Energy Conversion*, *16*(3), 209–213.

Zerdali, E., & Barut, M. (2013). *MRAS based real-time speed-sensorless control of induction motor with optimized fuzzy-PI controller*. 2013 IEEE international symposium on sensorless control for electrical drives and predictive control of electrical drives and power electronics (SLED/PRECEDE). IEEE.

Zhang, R., Gu, F., Mansaf, H., Wang, T., & Ball, A. D. (2017). Gear wear monitoring by modulation signal bispectrum based on motor current signal analysis. *Mechanical Systems and Signal Processing*, *94*, 202–213.